Desalination and Water Treatment
www.deswater.com

doi: 10.5004/dwt.2017.21429

92 (2017) 116–127
October

Removal of trihalomethane precursors from water using activated carbon obtained from oak wood residue: kinetic and isotherm investigation of adsorption process

Ali Akbar Babaei[a,b], Ehsan Niknam[c,*], Amin Ansari[d], Kazem Godini[e]

[a]*Environmental Technologies Research Center, Ahvaz Jundishapur University of Medical Sciences, Ahvaz, Iran, Tel. +98 61 33738269; email: babaei-a@ajums.ac.ir (A.A. Babaei)*
[b]*Department of Environmental Health Engineering, School of Public Health, Ahvaz Jundishapur University of Medical Sciences, Ahvaz, Iran*
[c]*Department of Environmental Engineering, Khuzestan Science and Research Branch, Islamic Azad University, Ahvaz, Iran, Tel. +98 9171244200; email: eniknam67@gmail.com*
[d]*Department of Chemistry, Faculty of Science, University of Bu-Ali Sina, Hamadan 65174, Iran, Tel. +98 9365383934; email: aminansari138@yahoo.com*
[e]*Department of Environmental Health and Health Sciences Research Center, Hamedan University of Medical Sciences and Health Services, Hamadan, Iran, Tel. +98 9188373716; email: kgoodini@razi.tums.ac.ir*

Received 2 February 2017; Accepted 16 September 2017

ABSTRACT

A novel adsorbent, activated carbon prepared from oak wood residue (ACOWR) was applied to eliminate trihalomethanes (THMs) precursors in an improved adsorption process. The prepared adsorbent was characterized by the Brunauer–Emmett–Teller and Barrett–Joyner–Halenda surface area measurement, Fourier transform infrared spectroscopic and scanning electron microscopic analyses. Moreover, the impacts of parameters including pH value, initial total organic carbon (TOC) concentration, contact time and adsorbent dose on TOC and UV_{254} removal from water were surveyed. Both TOC adsorption efficiency and UV_{254} removal remained approximately constant within the pH range of around 3–8. At the optimal adsorption conditions: pH = 6.5 and contact time = 120 min, approximately 53% and 62% removal efficiencies were obtained, respectively, for TOC and UV_{254} removal using the adsorbent dose of 2.5 g L^{-1} and initial TOC concentration of 10 mg L^{-1}. Experimental data were fitted with different isotherms and kinetic models. The results showed that the adsorption data were fitted well to the Freundlich isotherm equations, indicating that THMs precursors' uptake was mainly directed by a heterogeneous physical adsorption. Also, the kinetic data were best fitted to the pseudo-second-order and intraparticle diffusion kinetic models. The results also showed that the preparation of the ACOWR is easy and can be employed as an adsorbent for the effective removal of THM precursors from aqueous environments.

Keywords: Oak wood activated carbon; Trihalomethane precursors; Adsorption kinetics; Adsorption isotherms

1. Introduction

Naturally present fulvic and humic acids, amino acids and other natural organic matter (NOM), as well as iodide and bromide ions in different water sources can react with chemical disinfectants used in water treatment and, in turn, form a range of disinfection by-products (DBPs) like the trihalomethanes (THMs). NOM is best described as a complex mixture of organic compounds: mainly humic acids (Fig. 1), fulvic acids and other organic compounds such as proteins, lipids, carbohydrates, carboxylic acids, amino acids and

* Corresponding author.

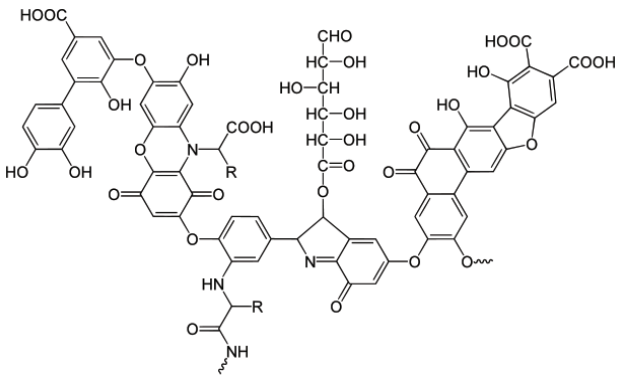

Fig. 1. Structure of humic acid.

hydrocarbons. Despite the key role of chlorine as the most common disinfectant worldwide in safe drinking water supplies, it leads to the formation of undesirable organic DBPs from reaction with NOM and bromide (Br^-) [1–8]. The two main classes of DBPs are THMs and haloacetic acids [9–11]. NOM is explained by two analyses: total organic carbon (TOC) and ultraviolet absorbance at wavelength of 254 (UV_{254}). Recently, reproductive consequences of THMs in drinking water like spontaneous abortion, stillbirth, and intrauterine growth reduction and harmful effects on liver, kidneys, bladder and central nervous system have been reported [12,13]. Moreover, various studies have claimed the formation and relevant health risks of THMs compounds [14–19].

The current regulations require water supply systems to eliminate or reduce THMs <80 μg L^{-1}. Based on the EPAs viewpoint, the best available technology to control THMs is removing the precursors in water treatment plants. Various treatment techniques have been employed to remove THMs precursors including coagulation–flocculation–sedimentation, adsorption with activated carbon, ion-exchange, electrocoagulation, biofiltration, membrane filtration, sonochemical process and advanced oxidation processes [20–28]. Adsorption is an effective well known water treatment process, which has been found to be superior to other water treatment methods in terms of cost-effectiveness, flexibility and simplicity of design, ease of operation and insensitivity to toxic pollutants. It does not result in the formation of harmful substances as well [29]. The application of adsorbents, as a filter media, leads to the optimization of the filtration process and, in turn, it maximizes the removal rate of the precursors [30,31]. Moreover, activated carbon filters are the most effective treatment system to be used at homes [29].

Various approaches have lately been investigated to develop cheaper and more effective adsorbents. Many nonconventional low-cost adsorbents including natural materials, biosorbents and agro-forestry wastes have been suggested by several researchers. These materials have the potential to be used as adsorbents for the removal of NOMs from aqueous solutions. However, unconventional adsorbents have been studied by many researchers to remove organic compounds from water and wastewater in terms of their cost-effectiveness, availability and adsorptive properties. Oak wood is a forest residue with great strength and hardness and is widely grown around the world, particularly in the Zagros Mountains in Iran. It has the potential to produce activated carbon with high adsorptive properties. Due to significant quantities of agro-forest and extensive use of oak wood, this study focused on the feasibility of applying activated carbon prepared from oak wood residue (ACOWR) as a low-cost adsorbent for TOC and UV_{254} removal from water.

The ACOWR adsorbents were prepared by using thermal process, characterized and applied for removing TOC and UV_{254} from the water. First, the optimum adsorption conditions were determined as a function of solution pH, contact time, initial concentration of TOC and UV_{254} and adsorbent dosage. Further, isotherms and kinetics were investigated and adsorption capacity of the ACOWR was evaluated.

2. Experimental

2.1. Materials and methods

All chemicals of the highest purity available including NaOH, H_3PO_4, HCl, KCl and potassium hydrogen phthalate (KHP) were purchased from Merck (Dermastat, Germany). The stock solution (200 mg L^{-1}) of TOC was prepared by dissolving 20 mg of the pure compound in 100 mL of double distilled water and the working solutions were prepared freshly. The pH values were measured by a lab pH meter (model-691; Metrohm, Switzerland) and the absorbance measurements were undertaken using a Jasco UV–Vis spectrophotometer (model V-530, Jasco, Japan) at 254 nm. The TOC values were measured by using a TOC analyzer (TOC-VCSH, Shimadzu Co., Japan). The morphology of the ACOWR was followed by field emission scanning electron microscopy (FESEM; Hitachi S-4160, Japan) under the acceleration voltage of 15 kV. A Brunauer–Emmett–Teller (BET) surface analyzer (Quantachrome NOVA 2000, USA) was employed to detect nitrogen adsorption–desorption isotherm at 77 K. Before each run, the samples were degassed through helium purging at 553 K for 3 h. The BET experiments give beneficial information on adsorbent characteristics like surface area, total pore volume and micropore area. These were performed to remove TOC and UV_{254}. This was done by adjusting the predicted batch concentration curves, obtained from the solution of the batch reactor model, to best-fit the experimental results. First, a 2-L flask was filled with 1.75 L of the raw water; then, appropriate amount of the activated carbon was added to the flask, and agitation was started. The quantity of the activated carbon was calculated using the following mass balance equations:

$$q_t = \frac{(C_0 - C_t)V}{M} \quad (1)$$

$$R = \frac{(C_0 - C_t)}{C_0} \times 100 \quad (2)$$

where C_0 is the initial TOC concentration (mg L^{-1}), C_t is the concentration of TOC at any time t, V is the volume of solution (L) and M is the mass of adsorbent (g). In this study, different conditions were examined as follows: contact time (2–150 min), pH (3–8), initial concentration (1, 5, 10 and 15 mg L^{-1}) and adsorbent dosage (0.5–5 g L^{-1}). All raw water samples were analyzed before starting the experiments.

A mixing speed of 300 rpm was found appropriate and consequently adopted for all batch experiments.

2.2. Preparation of ACOWR

The appropriate amount of the oak wood residue tree was cut to small parts and washed thoroughly and then was cooked and heated at 400°C in a 2.0 L vessel for 4 h. Subsequently, the oak wood was heated to boil in deionized water for over 2 h for removing water soluble phenol compounds and avoiding their release during the adsorption experiments. Next, the oak wood waste was washed with distilled water and dried at 150°C in an air-supplied oven for 12 h and then was grounded in a disk-mill and sieved (50–60 mesh). The carbonization process happened in argon atmosphere with heating rate of 5°C min^{-1} and the final temperature was set at 500°C and kept for 1 h [32]. The mass was then cooled and washed thoroughly a few times by distilled water and dried and fully characterized with different conventional techniques like scanning electron microscopy (SEM), Fourier transform infrared spectroscopy (FTIR), BET and Barrett–Joyner–Halenda (BJH) analyses.

3. Results and discussions

3.1. Characterization of ACOWR

The method of BJH is a procedure for calculating pore-size distributions from experimental isotherms, typically applied to nitrogen desorption data measured at 77 K on mesoporous materials. It uses the modified Kelvin equation to relate the amount of adsorbate removed from the pores of the material, as the relative pressure (P/P_0) is decreased from a high to low value, to the size of the pores.

The specific surface area of the ACOWR, based on BET surface area analyzer, was 73.612 m^2 g^{-1} and its pore-size distribution was calculated according to the nitrogen equilibrium adsorption isotherm at 77 K (Table 1). It was found that ACOWR possess a multimodal distribution of pores (the macropore and mesoporous domains). Pore diameters below 87.667 nm have total pore volume of <0.5 mL g^{-1} has abundance around 60%, that is, strongly high mesopore volume. The other part of pores between 100 and 200 nm has total volumes around 0.01523 cm^3 g^{-1} with frequency around 42% of the total pore volume that is known as macropores (Figs. 2 and 3). Also, the pore-size distribution calculated by the BJH method shows an average pore diameter of 157.352 Å (r_p = 78.5 Å) and BJH adsorption/desorption surface area of pores is 13.732 m^2 g^{-1} (Figs. 4 and 5). The FTIR spectra (Fig. 6) displayed some absorption peaks belonging to various functional groups or different vibration modes. The OH groups were seen in the range of 3,300–3,400 cm^{-1}, while the bands at about 2,923 cm^{-1} can be assigned to the aliphatic C–H groups, the peak at wave number of 1,701 cm^{-1} could be because of the carbonyl stretch of carboxyl. The trough around 1,605 cm^{-1} represented the C=O stretching. Also, the symmetric bending of CH_3 was seen to shift to around 1,382 cm^{-1} and the peaks at about 1,020 and 1,271 cm^{-1} support the presence of C–O stretching and SO_3 stretching of ether groups, respectively. The band around 1,605 cm^{-1} corresponds to the C=O stretching mode conjugated with the NH_2 (amide 1 band). The SEM micrograph of the adsorbent (×1.57 K magnification) has been presented in Fig. 7. The homogeneous structure and appearance of different pores in the adsorbent structure make it possible as useful sites for adsorption.

Table 1
Summary report of ACOWR

Surface area	
BET surface area	73.612 m^2 g^{-1}
BJH adsorption cumulative surface area of pores between 17 and 3,000 Å width	13.732 m^2 g^{-1}
BJH desorption cumulative surface area of pores between 17 and 3,000 Å width	1.4532 m^2 g^{-1}
Pore volume	
BJH adsorption cumulative volume of pores between 17 and 3,000 Å width	0.015231 cm^3 g^{-1}
BJH desorption cumulative volume of pores between 17 and 3,000 Å width	0.004123 cm^3 g^{-1}
Pore size	
Adsorption average pore width (4V/A by BET)	22.3211 Å
BJH adsorption average pore width (4V/A)	157.352 Å
BJH desorption average pore width (4V/A)	118.128 Å
Nanoparticle size	
Average particle size	876.673 Å

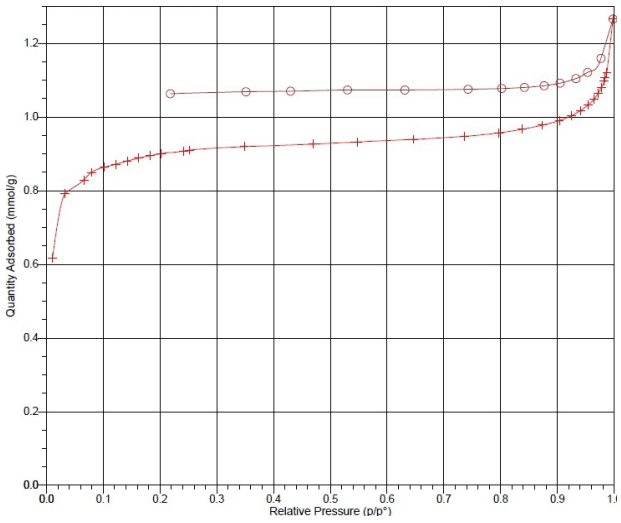

Fig. 2. Isotherm linear plot.

3.2. Effect of pH on TOC uptake

The pH parameter had an increasing impact on TOC removal through influencing adsorbents and adsorbate surface properties including charge, ionic structure and adsorption capacity [25]. Fig. 8 shows the effect of pH values on TOC adsorption onto the adsorbent at initial TOC

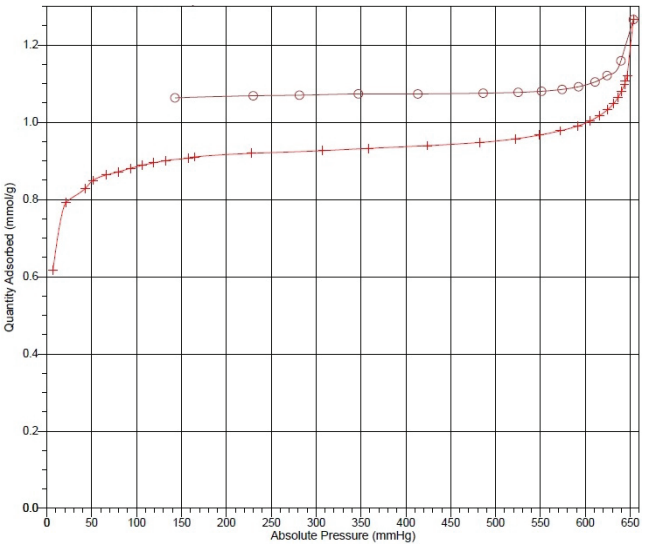

Fig. 3. Isotherm linear absolute plot.

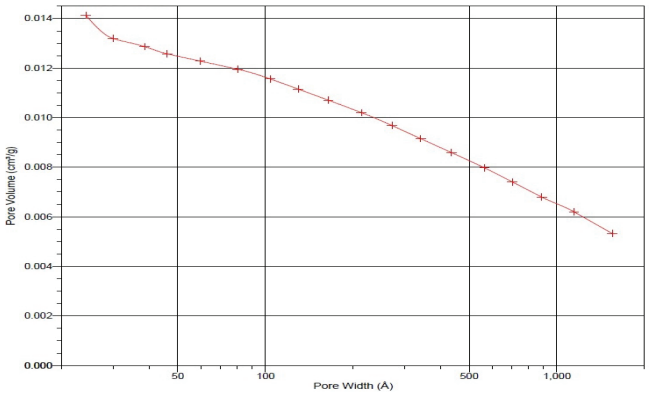

Fig. 4. BJH adsorption cumulative pore volume (larger) Halsey: Faas correction.

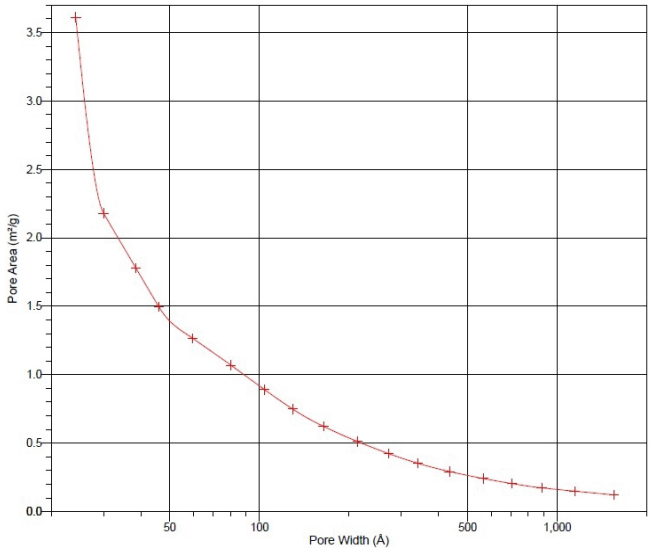

Fig. 5. BJH adsorption cumulative pore area (larger) Halsey: Faas correction.

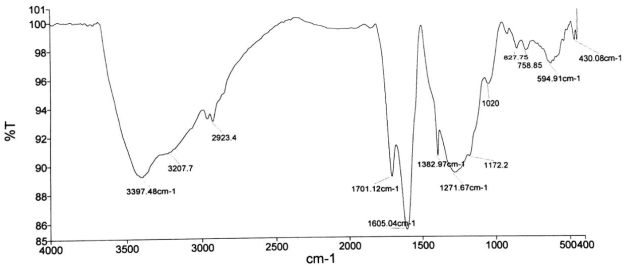

Fig. 6. FTIR study of ACOWR.

concentration of 10 mg L^{-1}, adsorbent dose of 2.5 g L^{-1} and contact time of 60 min. TOC adsorbed by the activated carbon was higher at high pH values. From Fig. 8, the optimum pH was attained at pH = 6.5. TOC removal increased dramatically with increasing pH solution until pH = 6.5. This may be attributed to the hydrophobic nature of the developed carbon which led to the adsorption of hydrogen ions (H^+) onto the surface of the carbon when immersed in water and made it positively charged. Low pH values (2.0–4.0) lead to an increase in H^+ ion concentration in the system and the surface of the activated carbon acquires positive charge by adsorbing H^+ ions. On the other hand, an increase in pH value (>5) led to increase in the number of negatively charged sites. As the ACOWR surface is negatively charged at high pHs, a significantly strong electrostatic attraction appears between the negatively charged carbon surface and THM precursors leading to maximum adsorption of TOC from water [25]. The lowest and highest adsorption occurred at pH 3.0 and ~6.5, respectively. Adsorbent surface would be positively charged up to pH < 3, and heterogeneous in the pH range 3–7. Thereafter, adsorbent surface should be negatively charged. Moreover, the increase of TOC adsorption with increasing pH value is also due to the attraction between THM precursors and excess OH^- ions in the solution.

3.3. Effect of adsorbent dosage

The amount of the adsorbent influenced significantly the adsorption efficiency and the vacant adsorption site of the adsorbent limited the rate and amount of migration of THMs precursors' molecule to the adsorbent surface. The effect of adsorbent amount on TOC and UV_{254} removal was studied by varying ACOWR dose from 0.5, 1.0, 2.5 and 5.0 g L^{-1} at pH 6.5 and at four different concentrations (1, 5, 10 and 15 mg L^{-1}) of TOC over various contact times at room temperature. As seen in Figs. 9(a) and (b), the number of vacant sites and concentration gradient improved significantly with increasing adsorbent dose. This high initial rate of adsorption with increasing adsorbent dose can be attributed to higher driving force and larger surface area. Subsequently, following the approximate saturation of adsorbent surface, the adsorption rate slowly raised and the possible and prominent mechanism is intraparticle diffusion for the sake of an increase in the number of pores and their volume [32–34]. By rising the adsorbent amount due to existence of high number of the reactive site with high tendency for interaction with various pathways is soft–soft interaction, π–π and hydrogen bonding improved significantly by electrostatic interaction. Therefore, a raise in

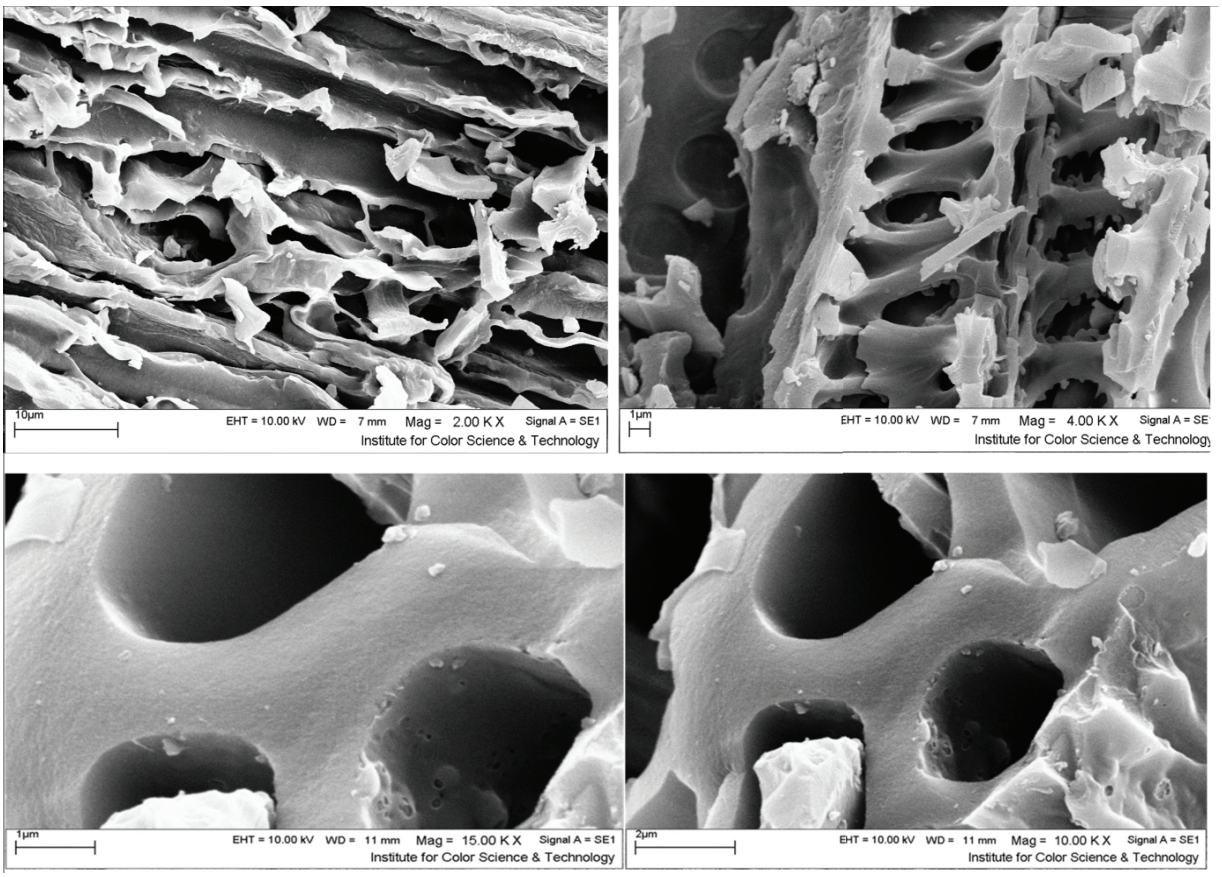

Fig. 7. FESEM images of the activated carbon oak wood.

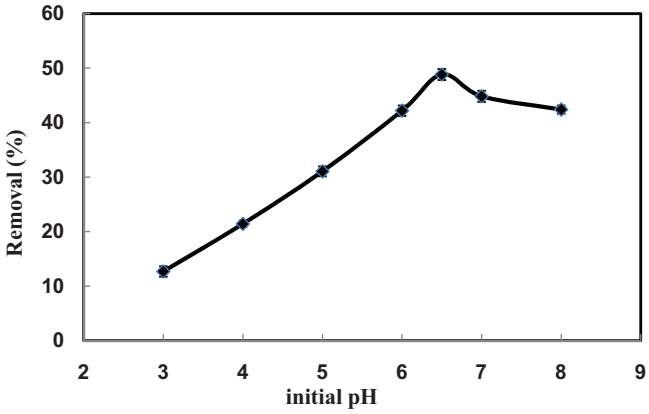

Fig. 8. Effect of solution pH on adsorption of TOC (10 mg L^{-1}) onto ACOWR (2.5 g L^{-1}) at room temperature (27°C ± 2°C), agitation speed 300 rpm for the contact time required to reach the equilibrium (60 min).

the adsorbent amount led to an increase in available surface area and adsorption sites and simultaneously increased the amount of mass transfer [26,27].

3.4. Effect of contact time

The study of the contact time variable contributes to better understanding the amount of the THMs precursors adsorbed at various time intervals by a fixed amount of the adsorbent. Equilibrium time is one of the most important factors for the design of economical water treatment systems [35]. The contact time necessary to reach equilibrium depends on the initial concentration of THMs precursors. Figs. 10(a) and (b) show the relationship between the THMs precursor removal and reaction time at various initial TOC concentrations, contact times (2–150 min), pH 6.5 and adsorbent doses 0.5–5.0 g L^{-1}. It was found that more than 30% of THMs precursors was removed during the first 60 min at all adsorbent dosages. The rapid THMs precursors' sorption at the initial stages of contact time could be attributed to the abundant availability of the active sites on the surface of these adsorbents. Afterwards, the reactive sites are occupied gradually, thereby reducing the sorption and removal efficiency [35]. The rapid adsorption at the initial contact time is emerged from the presence of more vacant reactive center leading to acceleration of mass transfer. At higher time, probably due to electrostatic repulsion between the adsorbed positive charges adsorbate onto the surface and the available THM precursors in the bulk cause a decrease in adsorption [28]. At higher concentration, due to a decrease in the ratio of TOC to ACOWR surface area, the rate of diffusion and migration significantly decreased.

3.5. Effect of initial TOC concentration

Initial TOC concentration provides an important driving force to overcome the mass transfer resistance of TOC

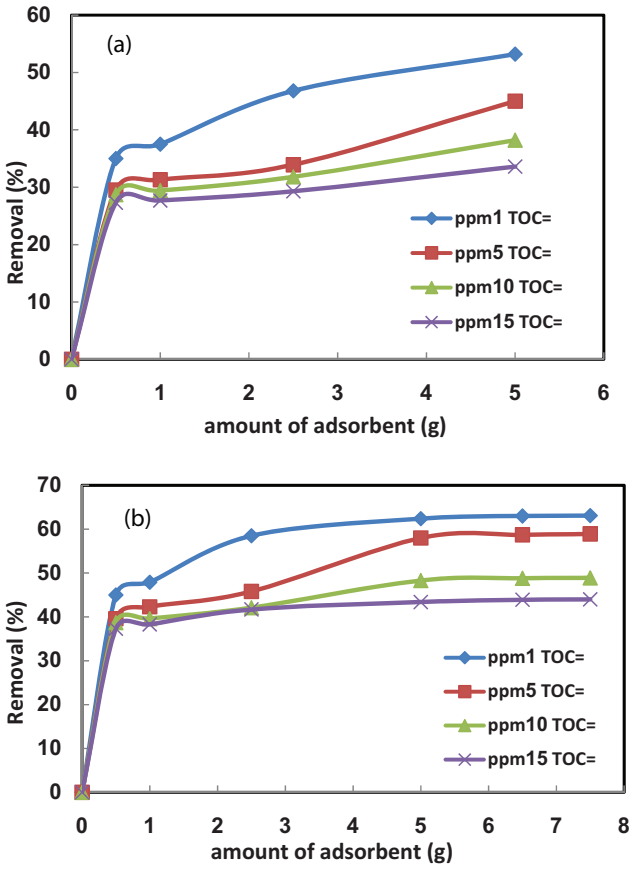

Fig. 9. Effect of adsorbent dosage (0.5–5.0 g L^{-1}) on removal of (a) TOC and (b) UV_{254} (pH 6.5, TOC concentrations of 1–15 mg L^{-1}).

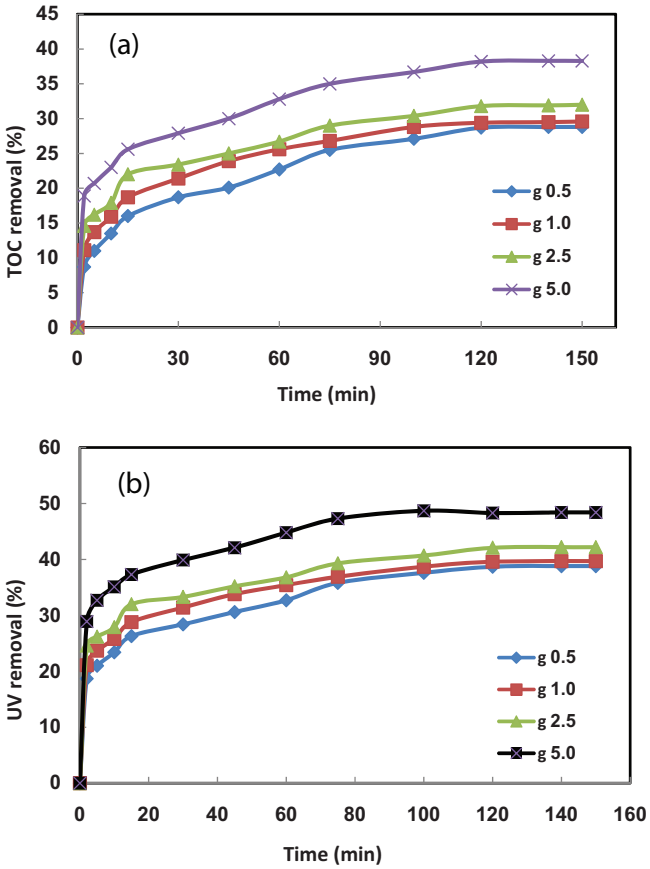

Fig. 10. Effect of contact time on removal of (a) TOC and (b) UV_{254} (adsorbent dosage 0.5–5.0 g L^{-1}, pH 6.5, TOC concentration 10 mg L^{-1}).

and UV_{254} in aqueous solutions. The effect of initial TOC concentration on removal efficiency was investigated at concentrations from 1 to 15 mg L^{-1} and adsorbent doses from 0.5 to 5.0 g L^{-1} (Figs. 11(a) and (b)). It was found that the actual amount of adsorbed TOC and UV_{254} on the adsorbent increased with raising their initial concentration and tended to attain saturation at higher concentrations [36]. With increasing initial TOC concentration, the percentage of TOC and UV_{254} removal decreased, while the actual amount of adsorbed TOC and UV_{254} increased. On the other hand, by increasing initial TOC concentration, the actual amount of TOC adsorbed per unit mass of the ACOWR increased. The higher initial concentration of TOC provides an important driving force to overcome the mass transfer resistance for TOC transfer between the solution and the surface of the ACOWR [29]. In the process, the THM precursors primarily encounter the boundary layer effect and then diffuse from boundary layer film onto adsorbent surface and finally diffuse into the porous structure of the adsorbent, which will take relatively longer contact time [37].

3.6. Adsorption isotherms

In order to optimize the design of an adsorption system for TOC removal, it is important to establish the most appropriate correlations for the equilibrium data for each system. Four isotherm models have been tested in the present study: Langmuir, Freundlich, Temkin and Dubinin–Radushkevich (D–R) models. The applicability of the isotherm equations is compared by judging the correlation coefficient, R^2.

3.6.1. Langmuir model

The Langmuir theory was based on this assumption that the adsorption was a type of chemical combination or process and the adsorbed layer was unimolecular. The theory can be represented by the following linear form [30,31]:

$$C_e/q_e = 1/Q_m k_a + C_e/Q_e \quad (3)$$

where C_e is the equilibrium concentration (mg L^{-1}), q_e is the amount adsorbed at equilibrium (mg g^{-1}) and Q_m (mg g^{-1}) and k_a (L mg^{-1}) are Langmuir constants related to adsorption capacity and energy of adsorption, respectively. The linear plots of C_e/q_e vs. C_e show that the adsorption obeys the Langmuir isotherm model for all adsorbents. The values of Q_m and k_a were determined for all adsorbents from intercept and slopes of the linear plots of C_e/q_e vs. C_e (Table 2). The good fit of the experimental data and the correlation coefficients (R^2) higher than 0.991 indicated the applicability of the Langmuir isotherm model. The essential characteristics of Langmuir dimensionless constant separation factor or equilibrium parameter, R_L, are defined by the following equation [38]:

$$R_L = 1/1 + k_a C_0 \quad (4)$$

where k_a (L mg^{-1}) is the Langmuir constant and C_0 (mg L^{-1}) is the initial concentration. The adsorption process can be considered as favorable when the R_L value ranges from 0 to 1. The values illustrate the isotherm to be either unfavorable (R_L < 1), linear (R_L = 1), favorable (0 < R_L <1) or irreversible (R_L = 0). On the other hand, an increase in R_L value with rising initial TOC concentration and adsorbent dosage showed high tendency of TOC for adsorption onto the ACOWR. In this research, the values of R_L (Table 2) were seen to be in the range of 0–1, illustrating that the adsorption process is favorable for the prepared activated carbon.

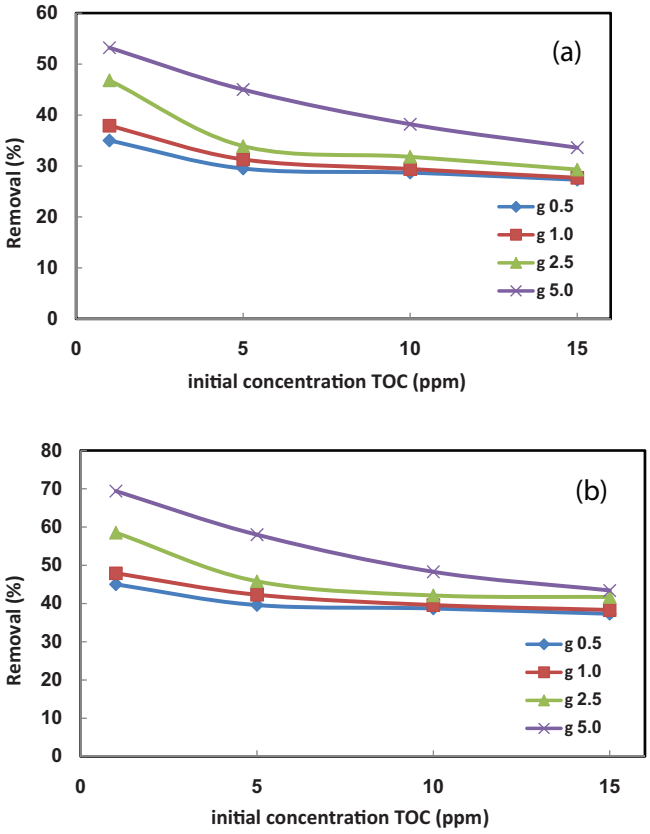

Fig. 11. Effect of initial TOC concentration on removal of (a) TOC and (b) UV_{254} (TOC concentration 1–15 mg L^{-1}, adsorbent dosage 0.5–5.0 g L^{-1}, pH 6.5).

3.6.2. Freundlich model

The Freundlich adsorption model stipulates that the ratio of solute adsorbed to the solute concentration is a function of the solution. The empirical model was shown to be consistent with an exponential distribution of active centers, characteristic of heterogeneous surfaces. The amount of solute adsorbed, q_e, is related to the equilibrium concentration of solute in solution, C_e, as follows:

$$q_e = K_F C_e^{1/n} \quad (5)$$

This expression can be linearized to give the following equation:

$$\ln q_e = \ln K_F + (1/n)\ln C_e \quad (6)$$

where K_F is a constant for the system, related to the bonding energy. K_F can be defined as the adsorption or distribution coefficient and respects the quantity of TOC adsorbed onto the ACOWR adsorbents for a unit equilibrium concentration (a measure of adsorption capacity, mg g^{-1}). The slope $1/n$, ranging between 0 and 1, is a measure of adsorption intensity or surface heterogeneity, becoming more heterogeneous as its value gets closer to zero [39]. A value for $1/n$ below 1 indicates a normal Freundlich isotherm, while $1/n$ above 1 is indicative of cooperative adsorption [40]. By plotting $\ln(q_e)$ vs. $\ln(C_e)$,

Table 2
Isotherm constant parameters and correlation coefficients calculated for the TOC adsorption onto ACOWR

Adsorbent (g L^{-1})						
Isotherm	Equation	Parameters	0.5	1.0	2.5	5.0
Langmuir	$C_e/q_e = 1/k_a Q_m + C_e/Q_m$	Q_m (mg g^{-1})	2.81	1.12	0.345	0.175
		k_a (L mg^{-1})	0.036	0.052	0.089	0.131
		R_L	0.65–0.96	0.56–0.95	0.43–0.92	0.34–0.88
		R^2	0.8344	0.8948	0.8478	0.991
Freundlich	$\ln q_e = \ln K_F + (1/n)\ln C_e$	$1/n$	1.14	1.19	1.33	1.35
		K_F (L mg^{-1})	9.89	17.75	33.97	51.41
		R^2	0.9996	0.9999	0.9983	0.9956
Temkin	$q_e = \beta\ln\alpha + \beta\ln Ce$	β	0.248	0.124	0.049	0.028
		α (L mg^{-1})	1.61	1.74	2.17	2.61
		R^2	0.8919	0.9016	0.8954	0.9520
Dubinin and Radushkevich	$\ln q_e = \ln Q_s - K\varepsilon^2$	Q_s (mg g^{-1})	1.78	3.46	8.17	13.23
		K	4E–07	3E–07	3E–07	2E–07
		E (J mol^{-1}) = $1/(2K)^{1/2}$	1,118.03	1,290.99	1,290.99	1,581.14
		R^2	0.8859	0.8907	0.8742	0.9227

the values of K_F and $1/n$ are determined from the intercept and slope of the linear regressions (Table 2).

3.6.3. The Temkin isotherm

Temkin adsorption isotherm judgment for suitability of each model for the representation of methods applicability for explanation of experimental data is according to R^2 value. Although both Langmuir and Freundlich models have reasonable and acceptable R^2 value, it is assumed that heat is logarithmic relation in contrast to adsorption in the Freundlich equation. The Temkin isotherm has commonly been applied in the following form [23,41]:

$$q_e = RT/b \ln(AC_e) \quad (7)$$

The Temkin isotherm Eq. (7) can be simplified to the following equation:

$$q_e = \beta \ln\alpha + \beta \ln C_e \quad (8)$$

where $\beta = (RT)/b$, T is the absolute temperature in Kelvin and R is the universal gas constant, 8.314 J mol^{-1} K^{-1}. The constant β is related to the heat of adsorption [42,43]. The adsorption data were analyzed according to the linear form of the Temkin isotherm (Eq. (8)). The examination of the data showed that the Temkin isotherm is efficiently usable for fitting the TOC adsorption onto the ACOWR. The linear isotherm constants and coefficients of determination have been shown in Table 2. The heat of TOC adsorption onto the ACOWR was found to increase from 0.0284 to 0.2482 kJ mol^{-1} with a decrease in the ACOWR dose from 5.0 to 0.5 g L^{-1}. The correlation coefficients R^2 gained from the Temkin model were comparable with that gained for the Langmuir and Freundlich equations, describing the applicability of the Temkin model to the adsorption of TOC onto the ACOWR.

3.6.4. The Dubinin–Radushkevich isotherm

The D–R model was also used to estimate the porosity, free energy and the properties of the adsorbents [44,45]. The D–R isotherm does not assume a homogeneous surface or constant adsorption potential. It has commonly been applied in the following Eq. (9) and its linear form can be shown in Eq. (10):

$$q_e = Q_s \exp(-K\varepsilon^2) \quad (9)$$

$$\ln q_e = \ln Q_s - K\varepsilon^2 \quad (10)$$

where K is a constant related to the adsorption energy, Q_s is the theoretical saturation capacity and ε is the Polanyi potential, calculated from Eq. (11).

$$\varepsilon = RT \ln(1 + 1/C_e) \quad (11)$$

The slope of the plot of $\ln q_e$ vs. ε^2 gives K (mol^2 kJ^{-2}) and the intercept yield the adsorption capacity, Q_s (mg g^{-1}). The mean free energy of adsorption (E), for transfer of 1 mol of target from infinity in solution to the surface of the solid was calculated from the K value using the following equation [46]:

$$E = 1/\sqrt{2K} \quad (12)$$

The calculated value of D–R parameters has been given in Table 2. The desorption capacity at optimum conditions using different amounts of adsorbents in the range of 13.23–1.78 mg g^{-1} has good agreement with respect to Langmuir value 2.81 mg g^{-1}. The values of E calculated using Eq. (12) were 1.581–1.118 kJ mol^{-1}, corresponding to physicosorption process playing a significant role in the adsorption of TOC onto the ACOWR.

3.7. Kinetic studies

Several steps can be used to examine the controlling mechanism of the adsorption process such as chemical reaction, diffusion control and mass transfer; kinetic models are used to test experimental data from the adsorption of TOC onto the ACOWR. The kinetics of pollutants adsorption onto the adsorbent is required for selecting optimum operating conditions for the full-scale batch process. The kinetic parameters, which are helpful for the prediction of adsorption rate, give important information for designing and modeling the adsorption processes. Thus, the kinetics of pollutant adsorption onto adsorbent was analyzed using pseudo-first-order [40,41], pseudo-second-order [42], Elovich [43,44] and intraparticle diffusion [43,45] kinetic models. The conformity between experimental data and the model predicted values was expressed by the correlation coefficients (R^2, values close or equal to 1). The relatively higher value is the more applicable model to the kinetics of TOC adsorption onto the ACOWR. The pseudo-first-order model was explained by Lagergren [47]. In the first-order kinetic model, which is the earliest known equation describes the adsorption rate based on the adsorption capacity. The differential equation is generally expressed as follows [41]:

$$\frac{dq_t}{dt} = k_1(q_e - q_t) \quad (13)$$

where q_e and q_t are the adsorption capacity at equilibrium and at time t, respectively (mg g^{-1}), k_1 is the rate constant of the pseudo-first-order adsorption (L min^{-1}). Integrating Eq. (13) for the boundary conditions $t = 0 - t$ and $q_t = 0 - q_t$ gives:

$$\log(q_e/(q_e - q_t)) = k_1 t/2.303 \quad (14)$$

Eq. (14) can be rearranged to obtain the following linear form:

$$\log(q_e - q_t) = \log q_e - \frac{k_1}{2.303} t \quad (15)$$

In order to obtain the rate constants, the values of $\log(q_e - q_t)$ were linearly correlated with t by plot of $\log(q_e - q_t)$ vs. t to give a linear relationship from which k_1 and predicted q_e can be determined from the slope and intercept of the plot, respectively. The variation in rate should be proportional to the first power of concentration for strict surface adsorption. However, the relationship between initial

solute concentration and rate of adsorption will not be linear when pore diffusion limits the adsorption process. The pseudo-first-order equation fits well for the first 30 min and thereafter the data deviate from theory. Thus, the model represents the initial stages where rapid adsorption occurs well but cannot be applied for the entire adsorption process. Furthermore, the correlation coefficients are relatively low (R^2 < 0.8999) for most adsorption data (Tables 3–6). This shows that the adsorption of TOC onto the ACOWR cannot be applied and the reaction mechanism is not a first-order reaction. The adsorption kinetic may be described by the pseudo-second-order model [42,48,49]. The differential equation is generally given as follows:

$$\frac{dq_t}{dt} = k_2(q_e - q_t)^2 \quad (16)$$

where k_2 (g mg^{-1} min^{-1}) is the second-order rate constant of adsorption. Integrating Eq. (16) for the boundary conditions $q_t = 0 - q_t$ at $t = 0 - t$ is simplified as can be rearranged and linearized to obtain [48,49]:

$$\frac{t}{q_t} = \frac{1}{k_2 q_e^2} + \frac{t}{q_e} \quad (17)$$

The second-order rate constants were used to calculate the initial sorption rate, given by the following equation:

$$h = k_2 q_e^2 \quad (18)$$

If the second-order kinetics is applicable, then the plot of t/q_t vs. t should show a linear relationship. Values of k_2 and equilibrium adsorption capacity q_e were calculated from the intercept and slope of the plots of t/q_t vs. t. The linear plots of t/q_t vs. t show good agreement between experimental and calculated q_e values at different initial TOC concentrations and adsorbent doses (Tables 3–6). The correlation coefficients for the second-order kinetic model are greater than 0.9985, which led to believe that the pseudo-second-order kinetic model provided good correlation for the adsorption of different initial contents of TOC onto the adsorbent. The values of initial sorption (h), which represent the rate of initial adsorption, are practically raised from 0.007 to 0.059 mg g^{-1} min^{-1} with an increase in initial TOC concentrations from 1.0, 5.0, 10.0 and 15.0 mg L^{-1} onto ACOWR dose 0.5 g L^{-1}. The Elovich equation as another rate equation based on the adsorption capacity in linear form has been successfully employed for the adsorption of solutes from a liquid solution [50,51]. The differential equation is generally explained as follows:

$$dq_t/dt = \alpha \exp(-\beta q_t) \quad (19)$$

where β is the initial adsorption rate (mg g^{-1} min^{-1}) and α is the desorption constant (g mg^{-1}) during any experiment. It is simplified by assuming $\alpha\beta_t >> t$ and applying the boundary conditions $q_t = 0$ at $t = 0$ and $q_t = q_t$ at $t = t$, Eq. (19) becomes:

$$q_t = 1/\beta \ln(\alpha\beta) + 1/\beta \ln(t) \quad (20)$$

The parameters (1/β) and (1/β) ln(αβ) can be calculated from the slope and intercept of the linear plot of q_t vs. ln(t). The obtained high R^2 value of this model was 0.9868 for TOC initial concentration in the range of 1.0–15.0 mg L^{-1} for ACOWR adsorbent (Tables 3–6). The parameter 1/β is related to the number of sites available for adsorption, while (1/β) ln(αβ) is the adsorption quantity when ln$t$ is equal to zero. Adsorption quantity at 1 min is helpful in understanding the adsorption behavior of the first step. The adsorbate species are most probably transported from the bulk of the solution into the solid phase through intraparticle diffusion/transport process, which is often the rate-limiting step in many adsorption processes, especially in a rapidly stirred batch reactor [43,52]. Since TOC is probably transported from its aqueous solution to the ACOWR

Table 3
Kinetic parameters of TOC adsorption onto ACOWR (adsorbent dosage 0.5 g L^{-1}, TOC concentration 1–15 mg L^{-1}, pH 6.5 and contact time 0–150 min)

TOC concentration (mg L^{-1})					
Models	Parameters	1	5	10	15
First-order kinetic model:	k_1	0.043	0.041	0.038	0.028
$\log(q_e - q_t) = \log(q_e) - (k_1/2.303)t$	$q_{e,cal}$	15.8	4.7	1.5	1.1
	R^2	0.8861	0.9761	0.7599	0.7949
Second-order kinetic model:	k_2	0.309	0.212	0.125	0.077
$t/q_t = 1/k_2 q_e^2 + (1/q_e)t$	$q_{e,cal}$	0.074	0.311	0.605	0.872
	R^2	0.9973	0.9906	0.9910	0.9954
	h	0.007	0.029	0.046	0.059
Intraparticle diffusion	k_{dif}	0.0048	0.0202	0.0412	0.609
$q_t = K_{id}t^{1/2} + C$	C	0.0206	0.0883	0.1358	0.1683
	R^2	0.9896	0.9762	0.9891	0.9898
Elovich	β	87.72	20.33	6.89	1.01
$q_t = 1/\beta \ln(\alpha\beta) + 1/\beta \ln(t)$	R^2	0.9557	0.9775	0.9593	0.9496
Experimental data	$q_{e,exp}$	0.070	0.300	0.574	0.820

Table 4
Kinetic parameters of TOC adsorption onto ACOWR (adsorbent dosage 1.0 g L^{-1}, TOC concentration 1–15 mg L^{-1}, pH 6.5 and contact time 0–150 min)

TOC concentration (mg L^{-1})					
Models	Parameters	1	5	10	15
First-order kinetic model:	k_1	0.053	0.046	0.040	0.036
$\log(q_e - q_t) = \log(q_e) - (k_1/2.303)t$	$q_{e,cal}$	36.08	8.04	3.49	2.65
	R^2	0.8639	0.8251	0.8467	0.8859
Second-order kinetic model:	k_2	3.209	0.802	0.357	0.238
$t/q_t = 1/k_2 q_e^2 + (1/q_e)t$	$q_{e,cal}$	0.039	0.161	0.308	0.440
	R^2	0.9918	0.9936	0.9935	0.9946
	h	0.005	0.021	0.034	0.046
Intraparticle diffusion	k_{dif}	0.002	0.009	0.019	0.029
$q_t = K_{id}t^{1/2} + C$	C	0.016	0.062	0.099	0.131
	R^2	0.9882	0.9567	0.9739	0.9667
Elovich	β	196.078	43.860	21.367	14.347
$q_t = 1/\beta \ln(\alpha\beta) + 1/\beta \ln(t)$	R^2	0.9618	0.9868	0.9840	0.9740
Experimental data	$q_{e,exp}$	0.038	0.157	0.294	0.416

Table 5
Kinetic parameters of TOC adsorption onto ACOWR (adsorbent dosage 2.5 g L^{-1}, TOC concentration 1–15 mg L^{-1}, pH 6.5 and contact time 0–150 min)

TOC concentration (mg L^{-1})					
Models	Parameters	1	5	10	15
First-order kinetic model:	k_1	0.049	0.043	0.040	0.036
$\log(q_e - q_t) = \log(q_e) - (k_1/2.303)t$	$q_{e,cal}$	5.832	8.685	18.978	86.198
	R^2	0.9191	0.7838	0.7665	0.7645
Second-order kinetic model:	k_2	1.4067	1.0521	0.4693	0.1149
$t/q_t = 1/k_2 q_e^2 + (1/q_e)t$	$q_{e,cal}$	0.0193	0.0693	0.1303	0.1815
	R^2	0.9980	0.9944	0.9910	0.9939
	h	0.003	0.010	0.016	0.023
Intraparticle diffusion	k_{dif}	0.001	0.004	0.007	0.010
$q_t = K_{id}t^{1/2} + C$	C	0.009	0.030	0.052	0.071
	R^2	0.9423	0.9704	0.9759	0.9662
Elovich	β	384.62	112.36	58.14	40.16
$q_t = 1/\beta \ln(\alpha\beta) + 1/\beta \ln(t)$	R^2	0.9793	0.9839	0.9597	0.9697
Experimental data	$q_{e,exp}$	0.0188	0.0678	0.1273	0.1758

by intraparticle diffusion; thus, the intraparticle diffusion is another kinetic model which should be applied to survey the rate of pollutant adsorption onto adsorbent. The possibility of intraparticle diffusion was explored by using the intraparticle diffusion model, which is commonly expressed by the following equation [45,52]:

$$q_t = k_{dif}t^{0.5} + C \quad (21)$$

where C (mg g^{-1}) is the intercept and k_{dif} is the intraparticle diffusion rate constant (mg g^{-1} $min^{-1/2}$). The values of q_t were found to be linearly correlated with values of $t^{1/2}$ and the rate constant k_{dif} directly evaluated from the slope of the regression line (Tables 3–6). The values of intercept C (Tables 3–6) provide explanation on the thickness of the boundary layer, the resistance to the external mass transfer increase as the intercept increase. The constant C was found to increase via increasing TOC concentration from 1.0 to 15.0 mg L^{-1}, indicating the increase in the thickness of the boundary layer and decrease of the chance of the external mass transfer and hence increase in the chance of internal mass transfer. The R^2 values given in Tables 3–6 are close to unity indicating the application of this model. This may confirm that the rate-limiting step is the intraparticle diffusion process. The intraparticle diffusion rate constant, k_{dif}, was in the range of 0.0048–0.609 mg g^{-1} $min^{-1/2}$ for 0.5 g L^{-1} of adsorbent and it increases with increase in the initial TOC concentration. This linear relationship shows high contribution of intraparticle diffusion on the adsorption process. Generally, in kinetic studies passing the intraparticle

Table 6
Kinetic parameters of TOC adsorption onto ACOWR (adsorbent dosage 5.0 g L^{-1}, TOC concentration 1–15 mg L^{-1}, pH 6.5 and contact time 0–150 min)

TOC concentration (mg L^{-1})					
Models	Parameters	1	5	10	15
First-order kinetic model:	k_1	0.054	0.045	0.043	0.041
$\log(q_e - q_t) = \log(q_e) - (k_1/2.303)t$	$q_{e,cal}$	11.06	11.53	32.24	180.51
	R^2	0.9518	0.8359	0.6787	0.7639
Second-order kinetic model:	k_2	20.534	3.676	1.649	1.279
$t/q_t = 1/k_2 q_e^2 + (1/q_e)t$	$q_{e,cal}$	0.011	0.046	0.078	0.103
	R^2	0.9985	0.9960	0.9912	0.9906
	h	0.002	0.008	0.010	0.014
Intraparticle diffusion	k_{dif}	0.0005	0.0023	0.0041	0.0053
$q_t = K_{id}t^{1/2} + C$	C	0.0058	0.0218	0.0332	0.0448
	R^2	0.9236	0.9527	0.9923	0.9940
Elovich	β	769.2	178.6	103.1	80.0
$q_t = 1/\beta \ln(\alpha\beta) + 1/\beta \ln(t)$	R^2	0.9794	0.9883	0.9535	0.9574
Experimental data	$q_{e,exp}$	0.011	0.045	0.076	0.101

diffusion plot through origin show that this mechanism solely limits the adsorption rate [45,52]. This condition was not obtained in the present research illustrating the contribution of other pathways besides intraparticle diffusion model to follow the adsorption data.

4. Conclusion

The powdered activated carbon adsorption process was found to be very effective in the removal of TOC and UV_{254} from aqueous solutions. This investigation illustrated the efficiency of the ACOWR as a good, green and low-cost adsorbent with a high adsorption capacity adsorbent (2.81 mg g^{-1}) for the removal of TOC from aqueous solutions. The effects of adsorbent dosage, initial pH, contact time and initial TOC concentration on TOC and UV_{254} removal were investigated via batch experiments. The optimum dosage, pH, initial concentration and contact time for the ACOWR were attained to be 2.5 g L^{-1}, 6.5, 10 mg L^{-1} and 120 min, respectively. Isotherm modeling revealed that the Freundlich equation could better explain the adsorption of TOC and UV_{254} onto the ACOWR as compared with other models. Kinetic data were appropriately fitted with the pseudo-second-order and Elovich adsorption rates for the ACOWR. The present study concludes that the ACOWR can be employed as a low-cost adsorbent and an alternative to commercial activated carbons for the removal of TOC and UV_{254} from water.

Acknowledgments

This article derived from MSc degree thesis of Ehsan Niknam which was performed under supervision of Dr. Ali Akbar Babaei (PhD) at Environmental Technologies Research Center, Ahvaz Jundishapur University of Medical Sciences. The authors of this paper are sincerely grateful to Ahvaz Jundishapur University of Medical Sciences for their academic supports.

References

[1] J.C. Crittenden, R.R. Trussell, D.W. Hand, K.J. Howe, G. Tchobanoglous, MWH's Water Treatment: Principles and Design, John Wiley & Sons, Hoboken, New Jersey, 2012.
[2] A.D. Nikolaou, S.K. Golfinopoulos, T.D. Lekkas, M.N. Kostopoulou, DBP levels in chlorinated drinking water: effect of humic substances, Environ. Monit. Assess., 93 (2004) 301–319.
[3] A. Nikolaou, T. Lekkas, S. Golfinopoulos, Kinetics of the formation and decomposition of chlorination by-products in surface waters, Chem. Eng. J., 100 (2004) 139–148.
[4] A.D. Nikolaou, S.K. Golfinopoulos, T.D. Lekkas, Formation of organic by-products during chlorination of natural waters, J. Environ. Monit., 4 (2002) 910–916.
[5] H. Gallard, U. Von Gunten, Chlorination of natural organic matter: kinetics of chlorination and of THM formation, Water Res., 36 (2002) 65–74.
[6] P. Singer, Humic substances as precursors for potentially harmful disinfection by-products, Water Sci. Technol., 40 (1999) 25–30.
[7] P.C. Singer, A. Obolensky, A. Greiner, DBPs in chlorinated North Carolina drinking waters, J. Am. Water Works Assoc., 87 (1995) 83–92.
[8] J.J. Rook, Formation of haloforms during chlorination of natural waters, J. Water Treat. Exam., 23 (1974) 234–243.
[9] F. Frimmel, J. Jahnel, Formation of Haloforms in Drinking Water, Haloforms and Related Compounds in Drinking Water, Handbook of Environmental Chemistry, Springer-Verlag, Berlin Heidelberg, Germany, 2003, pp. 1–19.
[10] H. Arora, M.W. LeChevallier, K.L. Dixon, DBP occurrence survey, J. Am. Water Works Assoc., 89 (1997) 60–68.
[11] P.C. Singer, Control of disinfection by-products in drinking water, J. Environ. Eng., 120 (1994) 727–744.
[12] C. Legay, M.J. Rodriguez, J.B. Sérodes, P. Levallois, Estimation of chlorination by-products presence in drinking water in epidemiological studies on adverse reproductive outcomes: a review, Sci. Total Environ., 408 (2010) 456–472.
[13] M.B. Toledano, M.J. Nieuwenhuijsen, N. Best, H. Whitaker, P. Hambly, C. de Hoogh, J. Fawell, L. Jarup, P. Elliott, Relation of trihalomethane concentrations in public water supplies to stillbirth and birth weight in three water regions in England, Environ. Health Perspect., 113 (2005) 225–232.
[14] R.M. Clark, R.C. Thurnau, M. Sivaganesan, P. Ringhand, Predicting the formation of chlorinated and brominated by-products, J. Environ. Eng., 127 (2001) 493–501.

[15] D.D. Gang, R.L. SEGAR, T.E. Clevenger, S.K. Banerji, Using chlorine demand to predict TTHM and HAA9 formation, J. Am. Water Works Assoc., 94 (2002) 76–86.
[16] J. Sohn, G. Amy, J. Cho, Y. Lee, Y. Yoon, Disinfectant decay and disinfection by-products formation model development: chlorination and ozonation by-products, Water Res., 38 (2004) 2461–2478.
[17] H. Chang, H. Tung, C. Chao, G. Wang, Occurrence of haloacetic acids (HAAs) and trihalomethanes (THMs) in drinking water of Taiwan, Environ. Monit. Assess., 162 (2010) 237–250.
[18] A.R. Pardakhti, G.R.N. Bidhendi, A. Torabian, A. Karbassi, M. Yunesian, Comparative cancer risk assessment of THMs in drinking water from well water sources and surface water sources, Environ. Monit. Assess., 179 (2011) 499–507.
[19] S. Kumar, S. Forand, G. Babcock, S.-A. Hwang, Total trihalomethanes in public drinking water supply and birth outcomes: a cross-sectional study, Maternal Child Health J., 18 (2014) 996–1006.
[20] M.C. Lee, V.L. Snoeyink, J.C. Crittenden, Activated carbon adsorption of humic substances, J. Am. Water Works Assoc., 73 (1981) 440–446.
[21] W.J. Weber Jr., T.C. Voice, A. Jodellah, Adsorption of humic substances: the effects of heterogeneity and system characteristics, J. Am. Water Works Assoc., 75 (1983) 612–619.
[22] J.C. Crittenden, J.K. Berrigan, D.W. Hand, B. Lykins, Design of rapid fixed-bed adsorption tests for nonconstant diffusivities, J. Environ. Eng., 113 (1987) 243–259.
[23] P.S. Kim, J.M. Symons, Using anion exchange resins to remove THM precursors, J. Am. Water Works Assoc., 83 (1991) 61–68.
[24] H. Wang, X. Yuan, Z. Wu, L. Wang, X. Peng, L. Leng, G. Zeng, Removal of basic dye from aqueous solution using *Cinnamomum camphora* sawdust: kinetics, isotherms, thermodynamics, and mass-transfer processes, Sep. Sci. Technol., 49 (2014) 2689–2699.
[25] H. Wang, X. Yuan, G. Zeng, L. Leng, X. Peng, K. Liao, L. Peng, Z. Xiao, Removal of malachite green dye from wastewater by different organic acid-modified natural adsorbent: kinetics, equilibriums, mechanisms, practical application, and disposal of dye-loaded adsorbent, Environ. Sci. Pollut. Res. Int., 21 (2014) 11552–11564.
[26] Y. Wu, H. Luo, H. Wang, L. Zhang, P. Liu, L. Feng, Fast adsorption of nickel ions by porous graphene oxide/sawdust composite and reuse for phenol degradation from aqueous solutions, J. Colloid Interface Sci., 436 (2014) 90–98.
[27] L. Leng, X. Yuan, H. Huang, J. Shao, H. Wang, X. Chen, G. Zeng, Bio-char derived from sewage sludge by liquefaction: characterization and application for dye adsorption, Appl. Surf. Sci., 346 (2015) 223–231.
[28] L.J. Leng, X.Z. Yuan, H.Z. Huang, H. Wang, Z.B. Wu, L.H. Fu, X. Peng, X.H. Chen, G.M. Zeng, Characterization and application of bio-chars from liquefaction of microalgae, lignocellulosic biomass and sewage sludge, Fuel Process. Technol., 129 (2015) 8–14.
[29] M. Rafatullah, O. Sulaiman, R. Hashim, A. Ahmad, Adsorption of methylene blue on low-cost adsorbents: a review, J. Hazard. Mater., 177 (2010) 70–80.
[30] A. Kara, E. Demirbel, N. Tekin, B. Osman, N. Beşirli, Magnetic vinylphenyl boronic acid microparticles for Cr(VI) adsorption: kinetic, isotherm and thermodynamic studies, J. Hazard. Mater., 286 (2015) 612–623.
[31] A. Kara, Adsorption of Cr(VI) ions onto poly(ethylene glycol dimethacrylate-1-vinyl-1,2,4-triazole), J. Appl. Polym. Sci., 114 (2009) 948–955.
[32] M. Ghaedi, A. Ghaedi, E. Negintaji, A. Ansari, A. Vafaei, M. Rajabi, Random forest model for removal of bromophenol blue using activated carbon obtained from *Astragalus bisulcatus* tree, J. Ind. Eng. Chem., 20 (2014) 1793–1803.
[33] A. Jain, V. Gupta, A. Bhatnagar, Suhas, A comparative study of adsorbents prepared from industrial wastes for removal of dyes, Sep. Sci. Technol., 38 (2003) 463–481.
[34] V.K. Gupta, R. Jain, M. Shrivastava, A. Nayak, Equilibrium and thermodynamic studies on the adsorption of the dye tartrazine onto waste "coconut husks" carbon and activated carbon, J. Chem. Eng. Data, 55 (2010) 5083–5090.
[35] R. Liu, B. Zhang, D. Mei, H. Zhang, J. Liu, Adsorption of methyl violet from aqueous solution by halloysite nanotubes, Desalination, 268 (2011) 111–116.
[36] M. Ghaedi, A. Ansari, M. Habibi, A. Asghari, Removal of malachite green from aqueous solution by zinc oxide nanoparticle loaded on activated carbon: kinetics and isotherm study, J. Ind. Eng. Chem., 20 (2014) 17–28.
[37] M. Ghaedi, A. Ansari, R. Sahraei, ZnS:Cu nanoparticles loaded on activated carbon as novel adsorbent for kinetic, thermodynamic and isotherm studies of Reactive Orange 12 and Direct yellow 12 adsorption, Spectrochim. Acta, Part A, 114 (2013) 687–694.
[38] T.W. Weber, R.K. Chakravorti, Pore and solid diffusion models for fixed-bed adsorbers, AIChE J., 20 (1974) 228–238.
[39] F. Haghseresht, G. Lu, Adsorption characteristics of phenolic compounds onto coal-reject-derived adsorbents, Energy Fuels, 12 (1998) 1100–1107.
[40] K. Fytianos, E. Voudrias, E. Kokkalis, Sorption–desorption behaviour of 2,4-dichlorophenol by marine sediments, Chemosphere, 40 (2000) 3–6.
[41] X.S. Wang, Y. Qin, Equilibrium sorption isotherms for of Cu^{2+} on rice bran, Process Biochem., 40 (2005) 677–680.
[42] C. Pearce, J. Lloyd, J. Guthrie, The removal of colour from textile wastewater using whole bacterial cells: a review, Dyes Pigm., 58 (2003) 179–196.
[43] G. Akkaya, A. Özer, Biosorption of Acid Red 274 (AR 274) on *Dicranella varia*: determination of equilibrium and kinetic model parameters, Process Biochem., 40 (2005) 3559–3568.
[44] M. Dubinin, The potential theory of adsorption of gases and vapors for adsorbents with energetically nonuniform surfaces, Chem. Rev., 60 (1960) 235–241.
[45] M. Dubinin, Modern state of the theory of volume filling of micropore adsorbents during adsorption of gases and steams on carbon adsorbents, Zh. Fiz. Khim., 39 (1965) 1305–1317.
[46] L. Radushkevich, Potential theory of sorption and structure of carbons, Zh. Fiz. Khim., 23 (1949) 1410–1420.
[47] M. Ghaedi, A. Ansari, F. Bahari, A. Ghaedi, A. Vafaei, A hybrid artificial neural network and particle swarm optimization for prediction of removal of hazardous dye brilliant green from aqueous solution using zinc sulfide nanoparticle loaded on activated carbon, Spectrochim. Acta, Part A, 137 (2015) 1004–1015.
[48] D. Ruthven, K. Loughlin, The effect of crystallite shape and size distribution on diffusion measurements in molecular sieves, Chem. Eng. Sci., 26 (1971) 577–584.
[49] Y.S. Ho, G. McKay, Pseudo-second order model for sorption processes, Process Biochem., 34 (1999) 451–465.
[50] J.J. Pignatello, F.J. Ferrandino, L.Q. Huang, Elution of aged and freshly added herbicides from a soil, Environ. Sci. Technol., 27 (1993) 1563–1571.
[51] E. Bulut, M. Özacar, İ.A. Şengil, Adsorption of malachite green onto bentonite: equilibrium and kinetic studies and process design, Microporous Mesoporous Mater., 115 (2008) 234–246.
[52] M. Ghaedi, A.H. Jah, S. Khodadoust, R. Sahraei, A. Daneshfar, A. Mihandoost, M. Purkait, Cadmium telluride nanoparticles loaded on activated carbon as adsorbent for removal of sunset yellow, Spectrochim. Acta, Part A, 90 (2012) 22–27.